Local order and frustration in the geometrically frustrated spinels $Cd_{1-x}Zn_xV_2O_4$

Z. Zhang, Despina Louca, A. Visinoiu, and S.-H. Lee
Department of Physics, University of Virginia, Charlottesville, Virginia 22904, USA

J. D. Thompson, T. Proffen, and A. Llobet
Los Alamos National Laboratory, Los Alamos, New Mexico 87545, USA

Y. Qiu
NCNR, National Institute of Standards and Technology, Gaithersburg, Maryland 20899, USA
and Department of Materials Science and Engineering, University of Maryland, College Park, Maryland 20742, USA

S. Park
HANARO Center, Korea Atomic Energy Research Institute, Daejeon, Korea

Y. Ueda
Institute for Solid State Physics, University of Tokyo, Kashiwa, Chiba 277-8581, Japan
(Received 10 January 2006; revised manuscript received 5 May 2006; published 17 July 2006)

Orbitally degenerate frustrated spinels, $Cd_{1-x}Zn_xV_2O_4$, with $0 \leqslant x \leqslant 1$ were investigated using elastic and inelastic neutron scattering techniques. In the end members with $x=0$ and 1, a tetragonal distortion ($c<a$) has been observed upon cooling mediated by a Jahn-Teller distortion that gives rise to orbital ordering. This leads to the formation of spin chains in the *ab*-plane that upon further cooling, Néel ordering is established due to interchain coupling. In the doped compositions, however, the bulk susceptibility, χ, shows that the macroscopic transitions to cooperative orbital ordering and long-range antiferromagnetic ordering are suppressed. However, the inelastic neutron scattering measurements suggest that the dynamic spin correlations at low temperatures have similar one-dimensional characteristics as those observed in the pure samples. The pair density function analysis of neutron diffraction data shows that the local atomic structure does not become random with doping but rather consists of two distinct environments corresponding to ZnV_2O_4 and CdV_2O_4. This indicates that short-range orbital ordering is present which leads to the one-dimensional character of the spin correlations even in the low temperature cubic phase of the doped compositions.

DOI: 10.1103/PhysRevB.74.014108 PACS number(s): 78.70.Nx, 71.27.+a, 75.50.Ee

I. INTRODUCTION

The pyrochlore lattice made of a network of corner sharing tetrahedra has recently drawn considerable attention due to its rich properties ranging from magnetic frustration[1] to superconductivity.[2] When a magnetic ion resides at the vertices of the tetrahedral network and is governed by dominant nearest-neighbor antiferromagnetic (AFM) interactions, the spins alone cannot order at any temperature. In real systems, this lattice is realized in spinels, AB_2O_4, pyrochlores, AB_2O_7 and C15 Laves phases, AB_2. The insulating magnetic pyrochlores, AB_2O_7, usually undergo a spin-glass-like phase transition upon cooling as in the case of $Tb_2Mo_2O_7$.[3] On the other hand, the spinels and Laves phases usually undergo long-range magnetic ordering at low temperatures. More recently, the 3*d* spinels with t_{2g} electrons have been of interest because of their simple Hamiltonian that describes the dominant nearest-neighbor interactions due to direct overlap of the t_{2g} orbitals. An example is the case of $ZnCr_2O_4$ with half-filled t_{2g} orbitals where a spin-Peierls-like phase transition was observed and attributed to partially lifting the spin degeneracy.[4] Moreover, when the magnetic 3*d* ions are subject to orbital degeneracy as in the vanadate spinels, AV_2O_4, with A=Mg, Zn, and Cd, the orbital degree of freedom becomes important in determining the ground state properties of the system.

In the normal spinel structure, AV_2O_4, (A=Zn,Cd), the magnetic V^{3+} ($S=1$) ion is surrounded by oxygens octahedrally. The magnetic ions form the corner-sharing tetrahedral network. In ZnV_2O_4, a Jahn-Teller distortion induces the system to undergo a cubic to a tetragonal crystal structure transition while the magnetic correlations become one-dimensional due to orbital ordering as suggested theoretically by Ref. 5. Previous neutron scattering studies (Ref. 6) supported the orbital model proposed in Ref. 5: namely, the structural transition results from ordering of the d_{xy}, d_{yz}, and d_{zx} orbitals in a pattern that gives rise to the tetragonal anisotropy.[6] While in the cubic phase, all t_{2g} orbitals are equivalent and are randomly occupied by the two electrons, with cooling, the expansion of the lattice along the *ab*-plane lowers the energy level for the d_{xy} orbital. This orbital becomes a preferred orbital occupied by one electron while the other electron occupies one of the other two orbitals alternately along the *c*-axis giving rise to one-dimensional spin chains in the *ab* plane. A static and long-range magnetic ordering is observed when interchain coupling is established at a lower temperature.

The A site in spinel AV_2O_4 occupies the tetrahedral sites surrounded by four oxygens. When the A site is occupied by a nonmagnetic ion, it may be considered irrelevant to the magnetic properties of the system. However, in strongly correlated electron systems where the delicate balance for ac-

quiring a particular ground state depends on multiple competing interactions, the *A* site ion can directly affect the lattice topology of the magnetic ion and plays an important role to the selection criteria for the real ground state in a given compound. Given the degenerate nature of the geometrically frustrated spinels, the choice of one ground state over another will strongly depend on the subtle balance between the spin and other degrees of freedom such as lattice and orbital. In systems with different lattice or orbital energies, different physical properties have been observed. For instance, $ZnCr_2O_4$ has a *c*-axis contracted tetragonal distortion and commensurate magnetic order, while $CdCr_2O_4$ has a *c*-axis elongated tetragonal distortion and incommensurate magnetic order at low temperatures.[7] The difference is due to the different chemical pressures exerted by Cd and Zn that are quite different in size with nominal radii of 0.8 and 0.6 Å, respectively, in a four coordinated environment.[8] Studying the effects of chemical pressure on spinels would provide important information on how the spin, lattice, and orbital degrees of freedom are coupled to cope with the magnetic and/or orbital degeneracies in the systems.

In this paper, we report our studies on the effects of chemical pressure on the orbitally degenerate $Cd_{1-x}Zn_xV_2O_4$. The end members with $x=0$ and 1 undergo tetragonal lattice distortion and Néel ordering at low temperatures, whereas the doped systems undergo a transition to a spin-glass-like state only. We performed bulk susceptibility, elastic, and inelastic neutron scattering measurements on polycrystalline vanadate samples with several different Zn concentrations spanning the entire phase diagram. The focus is to study how the orbital degeneracy takes part in the physics of the frustrated vanadates by investigating the evolution of the local structure and spin correlations with changing chemical pressure. Our main results are as follows: (1) the $I(Q)$ line shape obtained on CdV_2O_4 is less asymmetric than the one observed in ZnV_2O_4. This may indicate that the antiferro orbital state is realized in ZnV_2O_4 whereas a ferri- or ferro-orbital state is realized in CdV_2O_4. (2) Although the Cd/Zn compounds do not undergo a structural transition and remain cubic at all temperatures, the inelastic neutron scattering intensity, $I(Q)$, becomes asymmetric in the momentum transfer, Q, at low temperatures. While the asymmetry is less than what is observed in the $I(Q)$ of the pure compounds in the tetragonal phase, it is still strikingly similar. (3) The pair density function (PDF) analysis of the neutron diffraction data shows that in the doped compounds the local environments around Zn and Cd ions are unique and correspond to ZnV_2O_4 and CdV_2O_4, respectively. The two findings imply that even though the cooperative long range orbital ordering observed in the end members is destroyed by the aperiodicity induced by the different Cd and Zn environments, *locally*, the doped compounds exhibit short-range orbital ordering. This is similar to the ordering observed in the pure compounds that leads to magnetic fluctuations with one-dimensional character as observed from the inelastic neutron scattering measurements.

II. METHODS

Polycrystalline samples except ZnV_2O_4 were prepared at the University of Virginia by the solid-state reaction method. The ZnV_2O_4 sample was prepared at the ISSP, University of Tokyo. Mixtures in proportional molar ratios of ^{114}CdO isotope, V_2O_3 (99.99% purity), and ZnO (99.9995% purity) were ground and pressed into pellets and sealed under vacuum in quartz tubes. The first annealing treatment was performed at 720° C for samples with high content of Cd ($x>0.5$) and at 800 °C for samples with high content of Zn ($x<0.5$) for about 60 h. A second annealing treatment was necessary in order to obtain a single phase. The high content Cd samples were mixed again with 0.1 g ^{114}CdO per 1 g of sample to compensate for the loss of Cd at high temperatures. Using the same procedure, the mixture was sealed under vacuum in quartz tubes and annealed at 1000 °C. The samples were characterized using a magnetic properties measuring system (MPMS) to determine their magnetic properties. About 3 g of polycrystalline sample of each compound was used in the neutron experiments. The use of ^{114}Cd eliminated the neutron absorption problem of natural Cd. The diffraction measurements were performed using the NPDF and HIPD diffractometers of the Los Alamos National Laboratory using the time-of-flight method at temperatures ranging from 300 to 13 K. The diffraction data were analyzed using the Rietveld refinement[9] to determine the crystal and magnetic structures. The refinement showed that about 2% of Cd vacancies are present in the pure CdV_2O_4. Chemical analysis was also performed by Galbraith Laboratories on select samples and found that they are close to stoichiometric compositions within 1% or 2%. The same diffraction data were used to determine the powder averaged total structure function, $S(Q)$. This was then Fourier transformed to obtain information on the local atomic structure using the pair density function (PDF) method of analysis.[10] The PDF provides real space information on the interatomic correlations. Details of this technique can be found in Ref. 11. The NPDF provides high momentum transfer, Q, data up to 50 $Å^{-1}$ that reduces termination errors in the PDF analysis as well as provides important information on the short-range correlations.

The inelastic measurements were performed using SPINS and DCS at the NIST Center for Neutron Research. The SPINS experiments were performed with an incident neutron energy of $E_i=5$ meV for the elastic measurements and with an $\hbar\omega=1$ meV for the inelastic measurements to obtain the order parameter as well as investigate the low temperature dynamics. Using the DCS we investigated the $x=1$ sample with an incident neutron energy of $E_i=28$ meV, and for the $x=0.7$ and 0.5 sample with an $E_i=15.5$ meV.

III. RESULTS AND DISCUSSION

A. Magnetic dynamics

1. Bulk susceptibility and phase diagram

The bulk susceptibility data, χ_{bulk}, obtained from powder samples of $Cd_{1-x}Zn_xV_2O_4$ from $x=0$ to 1 is shown as a function of temperature in Fig. 1. For $x=0$, CdV_2O_4, χ_{bulk} shows two distinct transitions, an upturn at ~85 K and a downturn at ~30 K.[12] For $x=1$, ZnV_2O_4, two distinct transitions are observed as well but with a downturn at ~50 K and another downturn at ~40 K.[13] Previous studies on ZnV_2O_4 showed

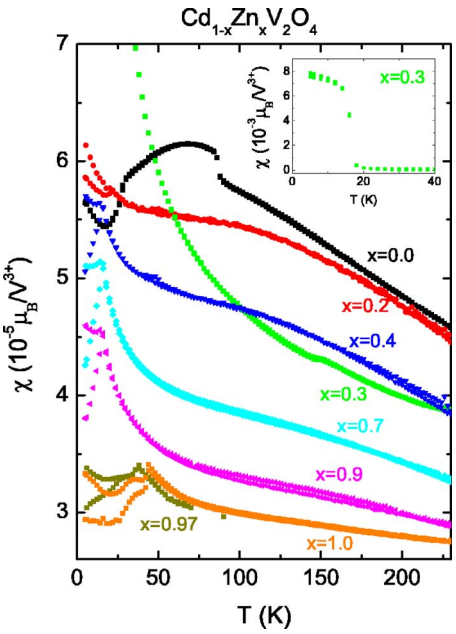

FIG. 1. (Color online) The bulk susceptibility, χ_{bulk}, as a function of temperature for $Cd_{1-x}Zn_xV_2O_4$. The inset shows χ_{bulk} of $x=0.3$ at low temperatures.

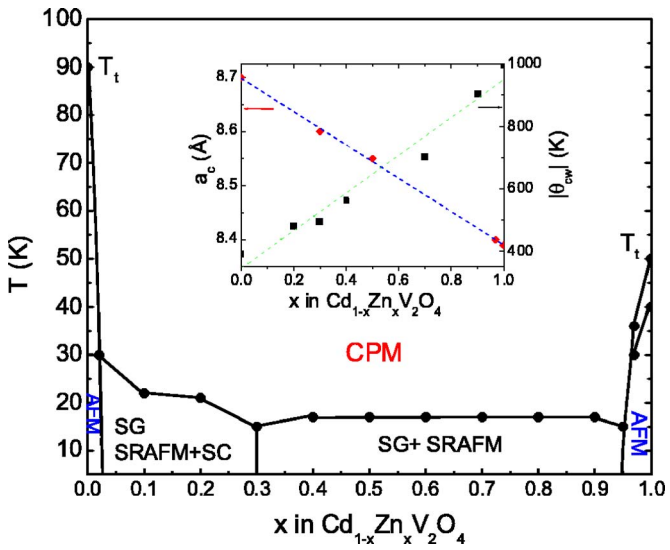

FIG. 2. (Color online) The phase diagram of $Cd_{1-x}Zn_xV_2O_4$. The magnetic and structural transition temperatures were obtained from χ_{bulk} and neutron data. T_t corresponds to the transition temperature to the tetragonal phase. A second transition to the AFM state is observed for the parent compounds, CdV_2O_4 and ZnV_2O_4, and for compositions with low doping at either end of the phase diagram. The intermediate compounds remain crystallographically cubic and undergo a transition to a spin-glass (SG) state. From the neutron data, additional short-range AFM (SRAFM) correlations were observed. For compositions with Zn doping up to about 30%, additional spin canting (SC) is observed. For temperatures above all transitions, all compounds are cubic and paramagnetic (CPM). The inset shows the approximate linear composition dependence of the cubic lattice constant and the Curie-Weiss, Θ_{CW}, temperature.

that the higher temperature transition is associated with a cubic to tetragonal structural distortion whereas the lower temperature transition is associated with a magnetic long-range Néel order.[6,13] With doping, the structural phase transition rapidly disappears; from the ZnV_2O_4 end, it only requires about 5% of Cd to completely suppress the transition while on the CdV_2O_4 end it takes less than 3% of Zn. The magnetic transition at lower temperature becomes spin-glass-like showing a field-cooled and zero-field-cooled hysteresis. The spin-glass phase shows a somewhat different behavior with composition: for $x \geqslant 0.4$, the system shows a clear spin-glass cusp in χ, whereas for $x \leqslant 0.4$, χ increases at low temperatures with cooling, most prominently displayed for $x=0.3$ which indicates a weak canted antiferromagnetic component. These results are summarized in the phase diagram of Fig. 2. Also shown in the inset of this figure is the extrapolated value of the Curie-Weiss temperature, Θ_{CW}, and the cubic lattice constant obtained from the neutron diffraction data as a function of composition. The Θ_{CW} was obtained by fitting the data within a narrow range with linear temperature dependence from 110 to 210 K. Even though the narrow temperature range used may introduce systematic errors on the absolute value of Θ_{CW}, it still shows the doping dependence of the Θ_{CW}. Θ_{CW} decreases with increasing Cd content while the lattice constant increases with Cd doping. This indicates that the nearest-neighbor interactions are dominant in these compounds due to direct overlap of neighboring t_{2g} orbitals whose strength is inversely proportional to the nearest-neighbor spacing.

2. *Magnetic neutron scattering of* CdV_2O_4 *and* ZnV_2O_4

In order to investigate the magnetic correlations in detail for the end members, elastic and inelastic neutron scattering measurements were performed. In Fig. 3(a), the elastic scattering data obtained from SPINS on CdV_2O_4 show that the low temperature phase corresponds to a magnetically ordered state with the same characteristic wave vector of $Q_M=(001)$ as the one observed in ZnV_2O_4.[6,14] The onset temperature for the magnetic ordering is ~30 K and is obtained from the temperature dependence of the $(100)_t$ magnetic peak shown in Fig. 3(b). The frozen moment, $1.19(3)\mu_B/V^{3+}$, is higher than the ordered moment of $0.63\mu_B/V^{3+}$ determined for ZnV_2O_4. The magnetic refinement of the diffraction data collected at HIPD indicates that the Zn and Cd systems have identical spin structures and corresponds to the one shown in Fig. 4. The magnetic cell is the same as the crystallographic unit cell and the magnetic ions form a collinear spin structure, marked by staggered AFM chains in the *ab*-plane and with an up-up-down-down $(+\ +\ -\ -)$ periodicity along the *c*-axis. The goodness of fit given by χ^2 is 3.23 for this model. Other models were tested with comparable χ^2 results: in particular, a model with up-up-down-down arrangement along the *c*-axis and with ferromagnetic coupling alternating direction in every other plane, interrupted by antiferromagnetic coupling sandwiched between ferromagnetic planes, gave rise to a χ^2 of 3.70. Both of these models yield different orbital ordering patterns and the choice of one over the other has to be accompanied by a particular orbital arrangement. The first model is consistent with the orbital model proposed by Ref. 5. Other spin struc-

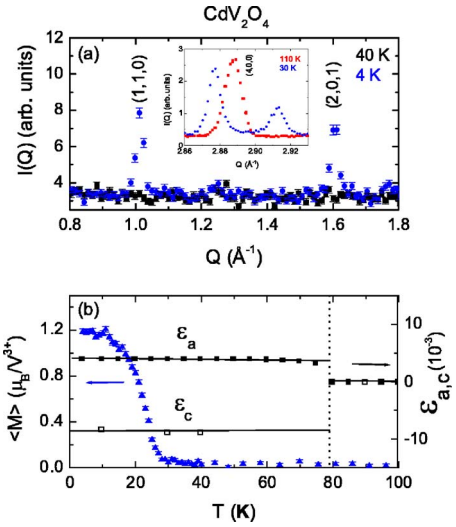

FIG. 3. (Color online) (a) Magnetic neutron scattering observed in CdV_2O_4 as a function of momentum transfer. Only the 4 K data show magnetic peaks. A cubic-tetragonal structural transition is observed at T_t=85 K evidenced by the splitting of the (4,0,0) nuclear peak (inset). (b) The CdV_2O_4 $(110)_c$ magnetic Bragg peak intensity (triangles) measured as a function of temperature shows the onset temperature for Néel order and coincides with the temperature observed in χ_{bulk}. The elastic strain (squares) along *a*- and *c*-axes changes close to T_t where this temperature coincides with the temperature where the first transition is observed in χ_{bulk}.

tures with more complex spin arrangements were tested that gave rise to worse results.

The tetragonal distortion occurs at a higher temperature than the Néel ordering as can be seen from the temperature dependence of the lattice strain along the *a*- and *c*-directions [Fig. 3(b)]. The lattice strain is evaluated using $\varepsilon_a = \frac{(a_t - a_c)}{a_c}$, where ε_a is the strain along the *a*-direction and a_t and a_c are the lattice constants in the tetragonal and cubic phases, respectively. The transition is marked by a contraction along the *c*-axis and an expansion along the *ab*-axis resulting in $c < a$. The transition can also be seen from the temperature dependence of the (400) nuclear peak in the inset of Fig.

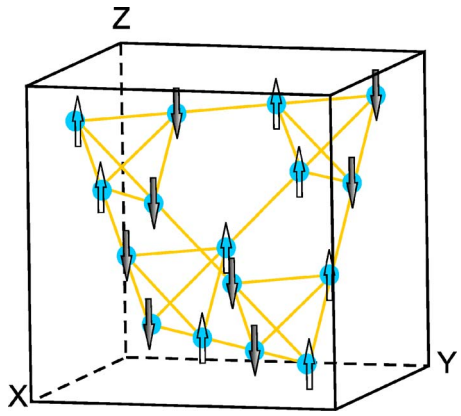

FIG. 4. (Color online) A model for the spin structure in CdV_2O_4. The V ions reside on the vertices of the tetrahedra. For simplicity, only the corner sharing tetrahedral network is shown.

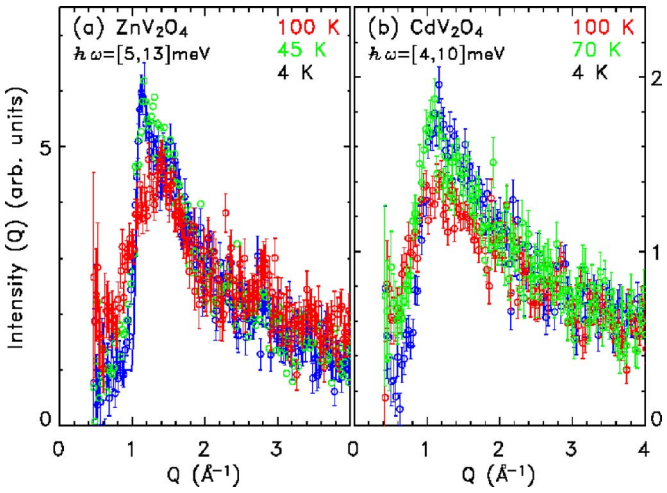

FIG. 5. (Color online) The energy integrated inelastic scattering intensity as a function of momentum transfer, *Q*. Limits of the integration incorporate the excitation area. In (a), data for ZnV_2O_4 at 100 (red), 45 (green), and 4 K (blue) are shown and correspond to the cubic paramagnetic, tetragonal paramagnetic, and tetragonal antiferromagnetic phases, respectively. In (b), data for CdV_2O_4 at 100, 70, and 4 K are shown. The similarity between the two sets of data indicates that the magnetic dynamics are similar in the two compounds.

3(a). This temperature is considerably higher than the structural transition temperature observed in ZnV_2O_4 (Ref. 13) and is related to the larger ion size of Cd in which case the lattice expands and becomes softer with Cd than with Zn. At the same time, the T_N is somewhat higher in ZnV_2O_4 than in CdV_2O_4 and this might be related to *J*, the coupling constant, which is weaker in CdV_2O_4 as estimated from the smaller Θ_{CW}.

Figure 5 is a plot of the energy integrated inelastic scattering intensity as a function of momentum transfer, *Q*, in the cubic paramagnetic, the tetragonal paramagnetic, and the tetragonal antiferromagnetic phases using the DCS spectrometer for the ZnV_2O_4 and CdV_2O_4 compounds. In the cubic phase (100 K) of ZnV_2O_4, the $I(Q)$ is symmetric around $Q = 1.3$ Å^{-1} while in CdV_2O_4, it is symmetric around $Q = 1.2$ Å^{-1}. The broad symmetric feature is expected in the case of isotropic correlations in three-dimensional space and their similarity indicates that the same kind of magnetic correlations are present in both systems. The difference in the *Q*-position of the peak is due to the difference in their lattice constants. Below the structural transition, the $I(Q)$ changes shape from symmetric to asymmetric characterized by a rapid decrease of the low *Q* portion of the data and a slow decrease at the higher *Q* end. The change in the line shape can be understood if the correlations contributing to the peak change from three-dimensional to a lower dimension.[6] The change in the line shape occurs when the lattice distorts to the tetragonal phase and indicates that the dynamic magnetic correlations are changing at temperatures higher than the long-range AFM transition. The anisotropic shape of the left of the peak in $I(Q)$ is very sharp in ZnV_2O_4 but less sharp in CdV_2O_4. This might be because the interchain coupling in ZnV_2O_4 is weaker and has more one-dimentional character-

istics than CdV_2O_4. This is consistent with the fact that the ordered moment of CdV_2O_4, 1.19 μ_B/V^{3+}, is greater than the moment of ZnV_2O_4 which is 0.63 μ_B/V^{3+}.

Such an asymmetric line shape can be understood if spin chains are present.[15] The structural and magnetic transitions can be explained by considering the orbital degree of freedom of the V^{3+} ($3d^2$) ions. In the cubic phase, the $3d$ orbitals split into t_{2g} and e_g states due to the octahedral crystal field. The two $3d$ electrons have an equal probability of occupying any two of the three t_{2g} orbitals. In the tetragonal phase ($c<a$), however, the d_{xy} orbital has a lower energy compared to the d_{zz} and d_{yz} orbitals and becomes one of the preferred orbitals occupied by one of the two electrons. The second electron then occupies one of the other two orbitals and the pattern of orbital occupancy by this second electron will affect the strength of the interchain coupling. In the *ab*-plane, the magnetic interaction between like orbitals becomes stronger because of direct orbital overlap. Consequently, the spins form AFM spin chains in the *ab*-planes. The long-range colinear structure is stabilized when out-of-plane interchain couplings become involved. The line shape of the powder inelastic $I(Q)$ reflects the strength of the interchain coupling and therefore the orbital state of the system. For instance, in the Motome and Tsunetsugu model, the second electron occupies the d_{xz} and d_{yz} alternately along the *c*-axis leading to very weak interchain coupling which is consistent with our neutron experimental data obtained on ZnV_2O_4. On the other hand two other orbital models have been proposed that give stronger interchain coupling and may explain the CdV_2O_4 data better; in the orbital model proposed by Khomskii and Mizokawa[16] the orbital occupancy for the second electron alternates between $d_{xz}-d_{xz}-d_{yz}-d_{yz}$ which makes the system an orthogonal spin ladder system. In the orbital model proposed by Tchernyshyov,[17] the second electron occupies the $d_{xz}+d_{yz}$ state that produces stronger interchain coupling.

3. Magnetic neutron scattering and average structure of doped compositions

With doping, the Rietveld refinement of the high resolution neutron diffraction data collected at NPDF showed no evidence of a structural transition and is consistent with the absence of a second transition in χ_{bulk}. The Néel ordered phase is replaced by a spin-glass-like phase with short-range spin correlations as indicated from the broad elastic Q dependence of the neutron $I(Q)$ intensity shown in Fig. 6 from data collected at SPINS for the $x=0.3$ sample. Gaussian fitting of the elastic peak yielded a correlation length of about 6 Å. This behavior is typical for compositions that exhibit a spin-glass-like phase. Although this sample shows a canted antiferromagnetic phase in χ_{bulk} results, the neutron results revealed short-range antiferromagnetic correlations with a broad elastic peak at 30 K, accompanied by a decrease of the low energy inelastic scattering intensity (Fig. 7). The onset temperature is higher than the transition temperature of 18 K observed in χ_{bulk} (see Figs. 1 and 2). This is common for systems that undergo spin freezing where depending on the instrumental resolution of the neutron experiment, quasielastic scattering events continuously shift to the elastic window throughout the transition. As a result, the transition temperature has a resolution dependence commonly observed in spin-glass systems[18,19] and in some of the cubic pyrochlores such as $Tb_2Mo_2O_7$.[20]

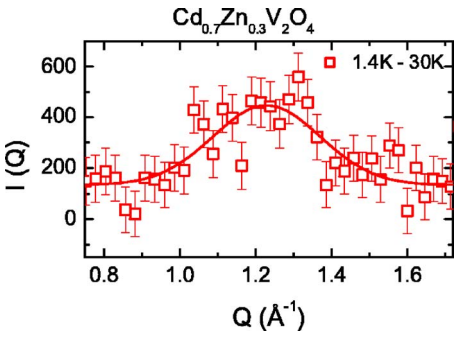

FIG. 6. (Color online) (a) Elastic neutron scattering intensity of $Cd_{0.7}Zn_{0.3}V_2O_4$ as a function of momentum transfer at 1.4 and 30 K. (b) Intensity difference between the two temperatures. The solid line is a guide to the eye.

Figure 8 shows the neutron inelastic intensity, $I(Q)$, for doped compositions $x=0.3$ and 0.5. At 100 K, the peak is symmetric as observed in the end members. At ~30–35 K, even though both samples do not undergo a structural transition, the $I(Q)$ line shape becomes asymmetric indicating that the dynamic spin correlations are changing where they become predominantly one dimensional at low temperatures. This suggests that the kind of orbital ordering scheme that is present in the pure compounds must be present in the doped compounds as well. But how can the magnetic dynamics of the cubic phases be similar to the dynamics of the tetragonal phase of the end members? And what kind of orbital ordering exists in the cubic phase of the doped compositions? To gain more insight into these issues, the local structure is discussed in the following section.

B. Local and global atomic structures

The diffraction data were analyzed with the Rietveld and PDF methods of analysis to compare the average crystallo-

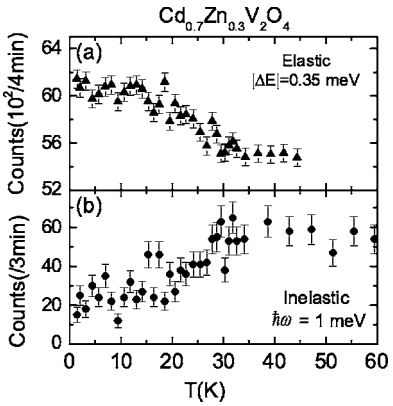

FIG. 7. (a) The temperature dependence of elastic intensity at $Q=1.2$ Å^{-1} for $x=0.3$ with $E_i=E_f=5$ meV. (b) The temperature dependence of inelastic intensity at $Q=1.2$ Å^{-1}. Upon lowering the temperature the elastic signal increases with an onset temperature of 30 K while the inelastic signal decreases. This temperature is higher than the transition temperature of 18 K observed in the bulk susceptibility.

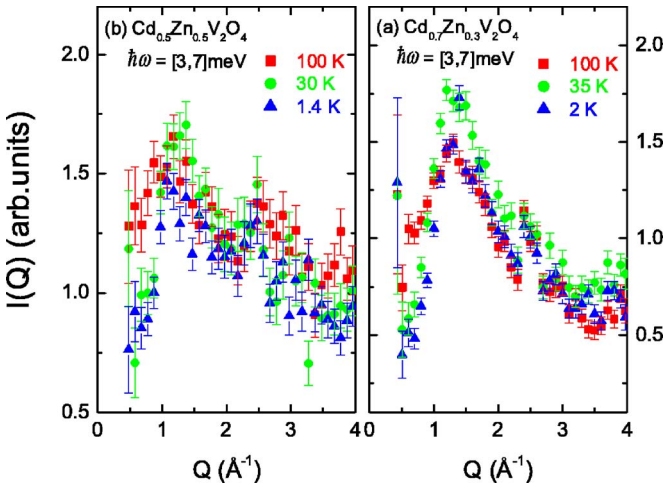

FIG. 8. (Color online) The energy integrated inelastic scattering intensity as a function of momentum transfer, Q. (a) Data for $Cd_{0.5}Zn_{0.5}V_2O_4$ at 100, 30, and 1.4 K are shown. (b) Data for $Cd_{0.7}Zn_{0.3}V_2O_4$ at 100, 35, and 2 K are shown. A similar line-shape change in the two doped compounds is observed as in the pure compounds.

graphic structure to the local atomic structure. The crystal symmetry for each compound synthesized is indicated on the phase diagram of Fig. 2. T_t corresponds to the cubic to tetragonal transition temperature which is only observed in the parent compounds and in compounds with small doping concentrations. All other compositions are cubic at all temperatures. The PDFs corresponding to the local atomic structure of ZnV_2O_4 and CdV_2O_4 determined from data collected at ~10 K are shown in Fig. 9. In ZnV_2O_4, the Zn-O and V-O correlations are close at 1.96 and 2.00 Å, respectively, and the superposition of the two peaks results in a positive peak. In the CdV_2O_4 PDF function, a small negative peak first appears at low r and corresponds to V-O octahedral correlations. It is negative and small because the coherent scattering length, b_c, for V ion is negative and small and the PDF is normalized by the b_c of each element. Since Cd is large, the Cd-O correlations are slightly longer than the V-O correlations and the two peaks are distinctly separate. The second peak corresponds to Cd-O correlations in the tetrahedral coordination. Following these features is a small peak around 2.4 Å that does not correspond to any known bond correlation in the tetragonal symmetry. At larger spacings are O-O correlations from the octahedral and tetrahedral sites. Note that the octahedral O-O bonds are split to short and long, centered around 2.6 and 3.1 Å, respectively, in CdV_2O_4 and around 2.73 and 2.97 Å in ZnV_2O_4.

The experimentally determined PDFs are compared to the model PDFs calculated from $\rho(r)=\frac{1}{4\pi Nr^2}\Sigma_{i,j}\frac{b_i b_j}{\langle b\rangle^2}\delta(r-r_{ij})$,[11] and using unit cell dimensions and atomic coordinates determined from Rietveld analysis as inputs to the models (Fig. 9). In both compounds, the crystallographic model (dashed line) agrees reasonably well with the experimentally determined local structure, especially in the case of ZnV_2O_4. Some discrepancies are observed between the model and experimentally determined PDF in CdV_2O_4 particularly around 2.4 Å. A second model labeled as the local model (solid line)

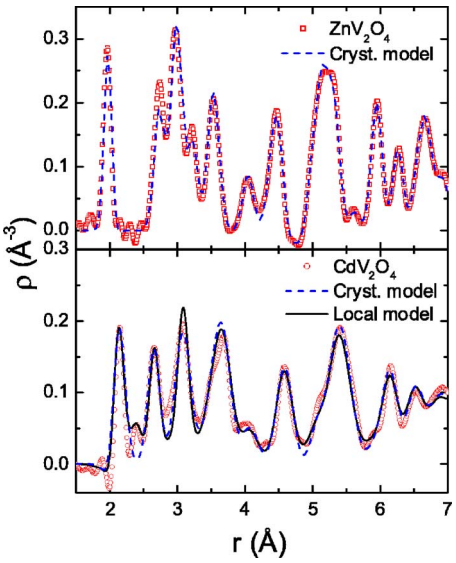

FIG. 9. (Color online) (a) The experimentally determined PDF corresponding to the local atomic structure of ZnV_2O_4 (open squares) is compared to the crystallographic model calculated from the atomic coordinates and unit cell dimensions obtained from Rietveld refinement (dashed line). (b) The PDF corresponding to the local atomic structure of CdV_2O_4 (open circles) is compared to two models: the crystallographic model (dashed line) with 2% Cd vacancies, and the local model (solid line) that considers Cd vacancies as well as oxygen distortions that propagate beyond the vacancies. The local model PDF is calculated using a $2\times2\times2$ cell. The oxygen ions close to the tetrahedral sites are displaced by as much as 0.3 Å. This reproduces the experimentally observed local environment quite well.

is shown in Fig. 9 (lower part) which provides a better agreement to the experimentally determined PDF in the vicinity of the 2.4 Å peak. This model takes into account tetrahedral distortions brought about by even one Cd ion missing and the consequences on the surrounding oxygen ions. The oxygen ions are distorted the most from their ideal positions closest to the vacancy and less as they get further away. The oxygen ions closest to Cd are displaced by as much as 0.3 Å. The local model provides a better agreement to the experimentally observed local structure in addition to reproducing the small peak at ~2.4 Å as can be seen from the figure.

The substitution of Cd with Zn suppresses the transition to the tetragonal phase as well as the AFM transition. The Rietveld analysis of the diffraction data of the doped compounds shows no evidence of a structural disorder associated with the difference in the Zn and Cd ion size. The crystal symmetry is cubic with Cd and Zn randomly distributed and sharing the same crystallographic sites. The Zn/Cd-O bonds yield only one bond-length value that shows a composition dependence as seen from Table I because the lattice expands with Cd doping. This result is in stark contrast to the local atomic structure that clearly shows two different peaks corresponding to the different Zn and Cd environments in the crystals. The PDFs corresponding to the local atomic structure of two samples with $x=0.3$ and 0.5 are shown in Fig. 10. Since the Zn and Cd ions nominal radii differ by ~0.2 Å, two types of bond lengths are observed *locally* correspond-

TABLE I. Zn/Cd-O and O-O bond lengths obtained from Rietveld and PDF analysis of the data as a function of composition. The O-O short and long bonds are from the octahedron. With increasing x, the short bonds get shorter and the long bonds get longer because of the pressure induced by the larger Cd ion.

	PDF (Å)		Rietveld (Å)	PDF (Å)		Rietveld (Å)	
x% Cd	Zn-O	Cd-O	Cd/Zn-O	Short O-O	Long O-O	Short O-O	Long O-O
0.0	1.96		1.95	2.736	2.969	2.730	2.977
0.5	1.95	2.14	2.049	2.710	3.016	2.698	3.03
0.7	1.94	2.14	2.082	2.682	3.026	2.684	3.052
1.0		2.14	2.14	2.663	3.070	2.656	3.089

ing to Zn-O and Cd-O pairs with a difference of 0.2 Å (the values are also listed in Table I). The first positive PDF peak corresponds to Zn-O at ~1.95 Å and the second one to Cd-O at ~2.15 Å. Zn and Cd have different b_c hence the amplitude of the two peaks is different, but it is clear that no peak is present at the position expected from the Rietveld refinement. As can be seen from Table I, these bond lengths remain largely unchanged with doping which serves as a clear indication that two distinct local environments are present.

Figure 11(a) is a plot of the local atomic structure corresponding to $Cd_{0.7}Zn_{0.3}V_2O_4$ that is compared to two models. In the crystallographic model (dashed line) from Rietveld analysis, the Zn-O and Cd-O peaks are not resolved since the Cd and Zn ions share the same site and yield one kind of average bond length. This usually leads to the assumption that the substitution induces randomness that destroys the tetragonal symmetry and the magnetic ordering. Locally, however, the atomic structure consists of two environments: those of ZnV_2O_4 and CdV_2O_4. This can be seen in the second model (solid line) where the two lattices are considered, one corresponding to Zn as in ZnV_2O_4 and its lattice constant, and another corresponding to Cd as in CdV_2O_4 and its lattice constant, with both units randomly distributed. This model agrees quite well with the experimentally determined PDF and reproduces the split corresponding to two types of local tetrahedral environments. The local structure differentiates between the Cd and Zn environments while the bond lengths between the ions in the local lattice closely resembles those found in the pure compositions. This model reproduces

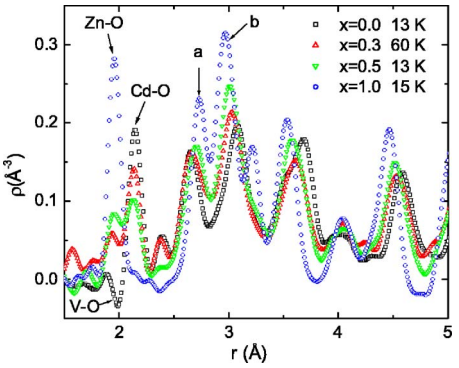

FIG. 10. (Color online) The PDFs corresponding to the local atomic structures for $Cd_xZn_{1-x}V_2O_4$ with $x=1$, 0.7, 0.5, and 0.0. The first negative peak corresponds to V-O pair correlations. The first positive peak corresponds to Zn-O bonds followed by the second peak corresponding to Cd-O pairs. In compounds containing Zn, the negative V-O peak is not visible because it overlaps with the more intense positive Zn-O peak and cancels out. For Cd/Zn containing compounds, two peaks are distinctly observed corresponding to Zn-O and Cd-O correlations at different distances. Following are the octahedral O-O pairs. They are separated to short (a) and long (b) bonds. A systematic shift of the O-O bonds is observed with the substitution of Zn for Cd due to the difference in the ion size between Cd and Zn. The local atomic structure for all these compounds ranging from one end of the phase diagram to the other is not very different. This indicates that the local symmetry is the same for all regardless of their long-range symmetry.

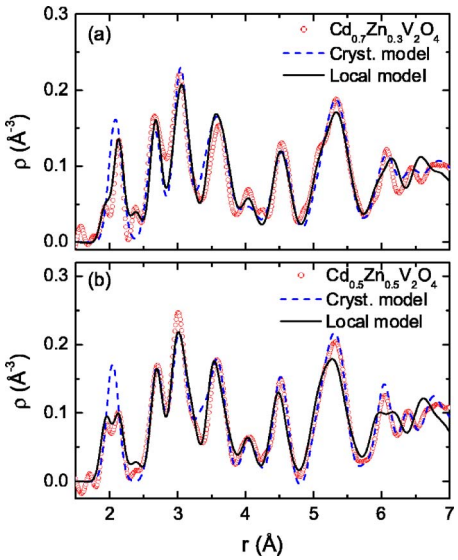

FIG. 11. (Color online) The PDFs corresponding to the local structure of (a) $Cd_{0.7}Zn_{0.3}V_2O_4$ and (b) $Cd_{0.5}Zn_{0.5}V_2O_4$ are compared to the crystallographic (dashed line) and local (solid line) models. Note that the crystallographic model does not reproduce the two distinct environments around Zn and Cd while the local model does. This is because in the cubic symmetry of the doped compounds, the Cd and Zn ions are not distinguished, although the lattice constant changes with doping. However, locally, two distinct environments are observed corresponding to Zn and Cd. At longer distances, the crystallographic model fits to the data better because the local differences are randomized and averaged out in the long range. This is not represented by the current local model as it is too simple and only uses one unit cell.

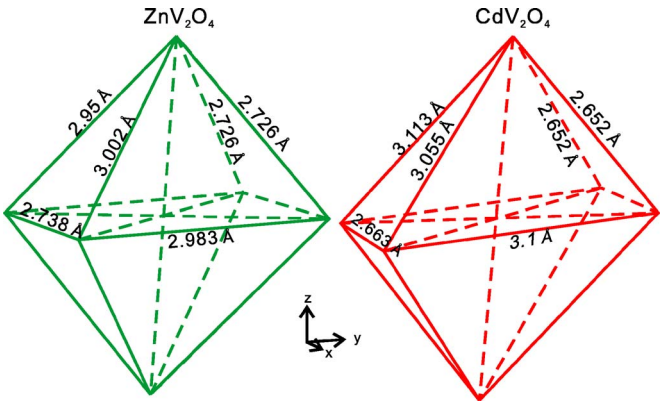

FIG. 12. (Color online) The VO_6 octahedral distortions as seen in ZnV_2O_4 and in CdV_2O_4. Due to the larger ion size of Cd, the distortion is greater in CdV_2O_4 than in ZnV_2O_4.

the short-range structure quite well, with some differences observed from 6 Å and above. This is to be expected because the model is simple; it consists of only one unit cell and cannot fully reproduce the long-range arrangements of the local distortions. Furthermore, the local atomic structure for $Cd_{0.5}Zn_{0.5}V_2O_4$ is compared to a model which is locally comprised of ZnV_2O_4 and CdV_2O_4 lattices (solid line) [Fig. 11(b)]. The agreement between this model and the experimental data is also very good. Also shown in this figure is the crystallographic model (dashed line). Due to the significant difference between Zn and Cd sizes, the PDF method of analysis identified the existence of the two environments in the doped samples.

The site disorder introduced by substituting Zn for Cd has a direct effect on the long-range magnetic interactions but very little, if any, on the local interactions. This is because the chemical pressure induced by the *A*-site ion distorts the VO_6 magnetic octahedra that subsequently affects the magnetic coupling and the extent of their orbital ordering. The distortion can be seen from Fig. 12 which is a plot of two octahedra, the left one with Zn at the *A* site and the right one with Cd at the *A* site. The vertices are occupied by O atoms and the O-O bond lengths were obtained both from the Rietveld and PDF analysis. As can be seen, different bond lengths result depending on whether a Zn or a Cd ion is in the vicinity. In pure compounds, since only one type of *A* ion is present, the octahedra are identical and can arrange themselves periodically over the entire lattice. In doped compounds, however, both kinds of octahedra are found which destroys any periodic arrangement over long distances. The composition dependence of the short and long O-O correlations are listed in Table I. As the Zn concentration increases, the bond-length difference between the short and long O-O bonds decreases, indicating a smaller octahedral distortion on average. This can be looked at from the Cd point of view as well when the Cd concentration increases, the difference between the two types of bond lengths increases because the Cd ion is bigger. With the octahedra changing shape from site to site orbital ordering is not allowed to propagate for long distances and for this reason the AFM long-range ordering is suppressed since no spin chains are formed. Thus doped systems do not undergo macroscopic transitions neither structurally nor magnetically. However, locally, short-range orbital ordering most likely exists as implied by the inelastic neutron data that show one-dimensional characteristics at low temperatures. This implies that locally, the local structure of the doped compositions is not cubic but rather tetragonal as in the pure compositions.

IV. CONCLUSION

The study of the local structure and magnetic dynamics of $Cd_{1-x}Zn_xV_2O_4$ presented in this paper has provided rich information directly related to the intricate interplay between orbital, spin, and lattice degrees of freedom. Due to the degenerate orbital degree of freedom of V^{3+} $(3d^2)$ ions, the pure ZnV_2O_4 and CdV_2O_4 undergo a tetragonal distortion upon cooling and leads to the one-dimensional characteristics of the magnetic correlations. Qualitative analysis indicates that different orbital states are realized in ZnV_2O_4 and CdV_2O_4. In the mixed compositions that show spin-glass-like behaviors at low temperatures, the tetragonal distortion disappears, however, the inelastic neutron scattering data, $I(Q)$, show asymmetric line shape which implies that similar orbital ordering as in the pure samples exists. Using a local structural technique of the pulsed neutron PDF analysis, we demonstrated that in the mixed compositions the local structure corresponds to the one found in the two pure samples. From all these data, we conclude that the local symmetry is tetragonal even in the mixed phase due to short-range orbital ordering, and leads to the asymmetric shape of $I(Q)$. The orbital ordering, however, cannot be propagated over the lattice in the doped compositions and therefore the long range structural and magnetic ordering do not occur.

ACKNOWLEDGMENTS

The authors would like to acknowledge valuable discussions with Y. Motome and D. I. Khomskii. Work at the University of Virginia is supported by the U. S. Department of Energy, under Contract No. DE-FG02-01ER45927, and the U.S. DOC through NIST-70NANB5H1152 at the Los Alamos National Laboratory under Contract No. W-7405-Eng-36. The use of the neutron scattering facilities at NIST was supported in part through NSF Grants No. DMR-9986442 and No. DMR-0086210.

[1] S.-H. Lee, C. Broholm, W. Ratcliff II, G. Gasparovic, T. H. Kim, Q. Huang, and S.-W. Cheong, Nature (London) **418**, 856 (2002).
[2] M. Hanawa, Y. Muraoka, T. Tayama, T. Sakakibara, J. Yamaura, and Z. Hiroi, Phys. Rev. Lett. **87**, 187001 (2001).
[3] J. S. Gardner, S. R. Dunsiger, B. D. Gaulin, M. J. P. Gingras, J. E. Greedan, R. F. Kiefl, M. D. Lumsden, W. A. MacFarlane, N. P. Raju, J. E. Sonier, I. Swainson, and Z. Tun, Phys. Rev. Lett. **82**, 1012 (1999).
[4] S.-H. Lee, C. Broholm, T. H. Kim, W. Ratcliff II, and S.-W. Cheong, Phys. Rev. Lett. **84**, 3718 (2000).
[5] H. Tsunetsugu and Y. Motome, Phys. Rev. B **68**, 060405(R) (2003); Y. Motome and H. Tsunetsugu, *ibid.* **70**, 184427 (2004).
[6] S.-H. Lee, D. Louca, H. Ueda, S. Park, T. J. Sato, M. Isobe, Y. Ueda, S. Rosenkranz, P. Zschack, J. Íñiguez, Y. Qiu, and R. Osborn, Phys. Rev. Lett. **93**, 156407 (2004).
[7] J.-H. Chung, M. Matsuda, S.-H. Lee, K. Kakurai, H. Ueda, T. J. Sato, H. Takagi, K.-P. Hong, and S. Park, Phys. Rev. Lett. **95**, 247204 (2005).
[8] R. D. Shannon, Acta Crystallogr., Sect. A: Cryst. Phys., Diffr., Theor. Gen. Crystallogr. **A32**, 751 (1976).
[9] A. C. Larson and R. B. VonDreele, Los Alamos National Laboratory Report No. LA-UR-86-748 (unpublished).
[10] B. H. Toby and T. Egami, Acta Crystallogr., Sect. A: Found. Crystallogr. **A48**, 33 (1992).
[11] D. Louca and T. Egami, Phys. Rev. B **59**, 6193 (1999).
[12] Similar data were previously reported by M. Onoda and J. Hasegawa, J. Phys.: Condens. Matter **15**, L95 (2003).
[13] Y. Ueda, N. Fujiwara, and H. Yasuoka, J. Phys. Soc. Jpn. **66**, 778 (1997).
[14] S. Niziol, Phys. Status Solidi A **18**, K11 (1973).
[15] G. Xu, J. F. DiTusa, T. Ito, K. Oka, H. Takagi, C. Broholm, and G. Aeppli, Phys. Rev. B **54**, R6827 (1996).
[16] D. I. Khomskii and T. Mizokawa, Phys. Rev. Lett. **94**, 156402 (2005).
[17] O. Tchernyshyov, Phys. Rev. Lett. **93**, 157206 (2004).
[18] J. A. Mydosh, *Spin Glasses* (Taylor and Francis, London, 1993).
[19] S.-H. Lee, Ph.D. thesis, The Johns Hopkins University, 1996.
[20] B. D. Gaulin, J. N. Reimers, T. E. Mason, J. E. Greedan, and Z. Tun, Phys. Rev. Lett. **69**, 3244 (1992).